J Appl Electrochem (2011) 41:423–433
DOI 10.1007/s10800-010-0252-1

ORIGINAL PAPER

Molecular modeling and electrochemical investigations of the corrosion inhibition of nickel using some thiosemicarbazone derivatives

K. F. Khaled

Received: 4 March 2010 / Accepted: 12 December 2010 / Published online: 5 January 2011

Abstract A relationship between molecular structures of three thiosemicarbazone derivatives and their inhibition capability was studied using electrochemical measurements (potentiodynamic polarization and EIS), molecular dynamics method and quantum chemical calculations. Electrochemical measurements results revealed that the inhibition efficiencies increased with the concentration of inhibitors. The molecular dynamic method results showed that the higher binding energy between the inhibitor and metal surface, the higher the adsorption energy and the higher the inhibition efficiency. Thiosemicarbazone derivatives have been simulated as adsorbate on Ni(111) substrate and the adsorption density, adsorption energy and binding energy have been identified on nickel surface.

Keywords Molecular modeling · Adsorption density · Binding energy · Acid corrosion

1 Introduction

With the advances in computer hardware and development of related theory, molecular modeling has grown to be an effective technique to explore complex systems at molecular level. Molecular structure, electron distribution and detailed adsorption process can be obtained via this approach, which is helpful for investigation of inhibition mechanism.

At the end of the twentieth century, much research based on molecular dynamics simulation was conducted to investigate the inhibitor mechanism on micro to mesoscopic scale [1–3]. The effect of corrosive environment factors, such as solvent, temperature and pressure, etc., on adsorption of inhibitor molecule on metal surfaces was also investigated. These research results have provided theoretical guidance for molecular design.

Nickel is one of the most important metals and is similar to iron in most of its properties. Common uses of nickel include production of stainless steel and other corrosion-resistant metals containing nickel [4, 5]. Nickel is also used in electroplating [6], electroforming [7] and sintered metal coatings [8]. The corrosion resistance of nickel is due to the formation of a passive film on its surface upon exposure to the corrosive media [9]. Nevertheless, nickel could be attacked by acidic media in a considerable rate. Thus, its corrosion rate must be controlled. The use of inhibitors is one of the most practical methods for protection against corrosion in acidic media [10].

Kumar et al. [11] studied the corrosion inhibition of nickel using different thiones in 4% nitric acid at different temperatures to determine the relative stability of the passive film formed on the nickel surface.

Khaled et al. [12, 13] studied corrosion and corrosion inhibition behavior of nickel electrode in 1.0 M HNO_3 in the absence and presence of several nitrogen and sulfur containing compounds. The results indicate a strong dependence of the inhibition performance on the nature of the metal surface, in addition to the structural effects of the inhibitors.

The aim of the present study is to investigate the inhibitive properties of three selected thiosemicarbazone derivatives, namely *p*-methoxyacetophenone thiosemicarbazone,

K. F. Khaled (✉)
Electrochemistry Research Lab, Chemistry Department, Faculty of Education, Ain Shams University, Roxy, Cairo, Egypt
e-mail: khaledrice2003@yahoo.com

K. F. Khaled
Materials and Corrosion Lab. (MCL), Chemistry Department, Faculty of Science, Taif University, Taif, Kingdom of Saudi Arabia

p-methylacetophenone thiosemicarbazone and *p*-aminoacetophenone thiosemicarbazone towards nickel corrosion in 1.0 M HNO_3 solutions using electrochemical techniques (polarization and impedance). It is also the objective of this study is to elucidate the adsorption behavior of the three selected thiosemicarbazone compounds on the nickel surface using quantum chemical calculation and molecular dynamics simulation techniques.

2 Experimental procedures

Experiments were carried out with 99.999% nickel electrode (Johnson Matthey Chemicals). The electrode was mounted in Teflon with an active flat disc shaped surface of (0.28 cm^2) geometric area to contact the test solution. Prior to each experiment the nickel electrode was abraded with different grit sizes emery papers up to 4/0 grit size to remove the corrosion products, if any, formed on the surface, cleaned in 18 MΩ water in an ultrasonic bath for 5 min and subsequently rinsed in acetone and bi-distilled water and immediately immersed in the test solution. The thiosemicarbazone derivatives used in this study were obtained from Aldrich Chemical co. and their molecular structures are as follow:

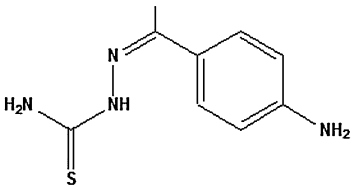

p-aminoacetophenone thiosemicarbazone

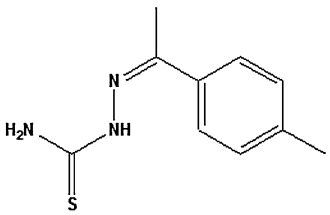

p-methylacetophenone thiosemicarbazone

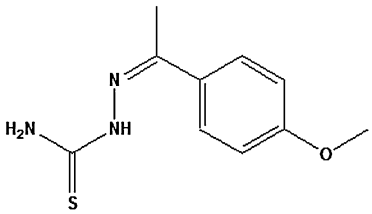

p-methoxyacetophenone thiosemicarbazone

They were added to the 1.0 M HNO_3 (Fisher Scientific) without pre-treatment at concentrations of 10^{-4}, 10^{-3}, 5×10^{-3}, and 10^{-2} M. The electrode was immersed in these solutions for 1 h before starting measurements.

Electrochemical measurements were carried out in a conventional electrochemical cell containing three compartments for Ni as working electrode, a platinum foil (1.0 cm^2) as counter electrode and a reference electrode. A Luggin capillary was also included in the design. The reference electrode was a saturated calomel electrode (SCE) used directly in contact with the working solution. The experiments were conducted in a 150 cm^3 volume cell, open to air, at 25 °C ± 1 using a temperature control water bath. All potential values were reported in volt (SCE).

Each run was carried out in stagnant aerated 1.0 M HNO_3 solutions without and with various concentrations (10^{-4}–10^{-2} M) of thiosemicarbazone derivatives. Polarization measurements were carried out starting from a cathodic potential of −0.27 V to an anodic potential of +0.2 V at a sweep rate of 0.1 mV s^{-1}. Impedance measurements were carried out using ac signals of amplitude 5.0 mV peak to peak at the open-circuit potential in the frequency range from 30 kHz to 1.0 mHz.

Measurements were performed with a Gamry Instrument Potentiostat/Galvanostat/ZRA. This includes a Gamry Framework system based on the ESA400, Gamry applications that include DC105 for dc corrosion measurements, EIS300 for impedance measurements to calculate the corrosion current and the Tafel constants along with a computer for collecting the data. Echem Analyst 5.58 software was used for plotting, graphing and fitting data.

3 Theoretical models and methods

The modeling studies were designed to examine thiosemicarbazone derivatives–surface interactions that lead to optimal molecular binding to the nickel surface. The studies would seek to compare the energy-minimized binding configurations as well as adsorption energies for the studied thiosemicarbazone derivatives. The nickel surface binding energies of these configurations were computed using $DMol^3$ [14], a high quality quantum mechanics computer program (available from Accelrys [14], San Diego, CA). These calculations employed an ab initio, local density functional (LDF) method with a double numeric polarization (DNP) basis set and a Becke-Perdew (BP) functional.

Molecular simulation studies were performed using Materials studio 5.0 software from Accelrys Inc [14] which has been used to build the thiosemicarbazone derivatives molecules, nickel surface (111) surface and solvent molecules using the sketching tools in Materials Visualizer. Molecular mechanics tools are used to investigate the Ni(111)/solvent/thiosemicarbazone derivatives systems. The key approximation is that the potential energy surface, on which the atomic nuclei move, is represented by a

classical forcefield. COMPASS (Condensed-phase Optimized Molecular Potentials for Atomistic Simulation Studies) [15], which used to optimize the structures of all components of the system of interest (Ni(111)/solvent/thiosemicarbazone derivatives) and represents a technology break-through in forcefield method. COMPASS is the first ab initio forcefield that enables accurate and simultaneous prediction of chemical properties (structural, conformational, vibrational, etc.) and condensed-phase properties (equation of state, cohesive energies, etc.) for a broad range of chemical systems. It is also the first high quality forcefield to consolidate parameters of organic and inorganic materials.

The first step in this computational study is the preparation of a model of molecules which adsorb on the surface with optimized geometry (i.e. energy minimized). Among the different steps involved in the modeling approach, is the construction of the Ni(111) surface from its pure crystal, the addition of the thiosemicarbazone derivatives near to the surface, the definition of the potentials (i.e. the forcefield) to study the liquid–solid interaction, followed by the geometry optimization calculation. This particular case, the use of molecular mechanics can be seen as a precursor to computationally more expensive quantum mechanical methods: once the model has been optimized with suitable forcefield (COMPASS), we will be able to simulate a substrate (Ni(111) surface) loaded with an adsorbate (i.e., the three selected thiosemicarbazone derivatives, taking into consideration the solvent effect. The objective of this computational study is to find low energy adsorption sites to investigate the preferential adsorption for the three selected thiosemicarbazone derivatives on Ni(111) surface aiming to find a relation between the effect of their molecular structure and their inhibition efficiency.

The MD simulation of the interaction between thiosemicarbazone derivatives and Ni(111) surface was carried out in a simulation box (14.33 × 14.33 × 19.650 Å) with periodic boundary conditions to model a representative part of the interface devoid of any arbitrary boundary effects. The Ni(111) was first built and relaxed by minimizing its energy using molecular mechanics, then the surface area of Ni(111) was increased and its periodicity is changed by constructing a super cell, and then a vacuum slab with 50 Å thicknesses was built on the Ni(111) surface. The number of layers in the structure was chosen so that the depth of the surface is greater than the non-bond cutoff used in calculation. Using five layers of nickel atoms gives a sufficient depth that the inhibitor molecules will only be involved in non-bond interactions with nickel atoms in the layers of the surface, without increasing the calculation time unreasonably. This structure then converted to have 3D periodicity. As 3D periodic boundary conditions are used, it is important that the size of the vacuum slab is great enough (50 Å) that the non-bond calculations for the adsorbate does not interact with the periodic image of the bottom layer of atoms in the surface. After minimizing the Ni(111) surface and thiosemicarbazone derivatives molecules, the corrosion system will be built by layer builder to place the inhibitor molecules on Ni(111) surface, and the behaviors of the these molecules on the Ni(111) surface were simulated using the COMPASS (condensed phase optimized molecular potentials for atomistic simulation studies) force field. Adsorption Locator module in Materials Studio 5.0 [14] have been used to model the adsorption of the inhibitor molecules onto Ni(111) surface and thus provide access to the energetic of the adsorption and its effects on the inhibition efficiencies of thiosemicarbazone derivatives [16]. The binding energy between thiosemicarbazone derivatives and Ni(111) surface were calculated using the following equation [17]:

$$E_{\text{binding}} = E_{\text{total}} - (E_{\text{surface}} + E_{\text{inhibitor}}) \quad (1)$$

where E_{total} is the total energy of the surface and inhibitor, E_{surface} is the energy of the surface without the inhibitor, and $E_{\text{inhibitor}}$ is the energy of the inhibitor without the surface.

4 Results and discussions

4.1 Electrochemical measurements

4.1.1 Electrochemical impedance spectroscopy

The experimental results obtained from EIS measurements for the corrosion of nickel in the presence and absence of thiosemicarbazone derivatives at 25 °C ± 1 are summarized in Table 1 and presented in Figs. 1, 2, and 3. Figures 1, 2, and 3 show the impedance spectra of nickel in 1.0 M HNO_3 solution in the absence and presence of different concentrations of thiosemicarbazone derivatives. As can be seen in Figs. 1, 2, and 3, for the methoxy and methyl derivatives, the complex impedance diagrams consist of three time constants, i.e., a large capacitive loop at high frequency (HF), a small capacitive loop at medium frequency (MF) and a small inductive one at low frequency (LF) values.

Moreover, the diameter of the large semicircle increases gradually with the increase of the thiosemicarbazone derivatives concentration from 10^{-4} to 10^{-2} M.

The HF capacitive loop is related to the charge transfer process of the metal corrosion and the double layer behavior, the LF inductive loop may be attributed to the relaxation processes obtained by adsorption of inhibitor on the electrode surface [18]. The inductive behavior at LF is

Table 1 Electrochemical parameters calculated from EIS measurements on nickel electrode in 1.0 M HNO_3 solutions without and with various concentrations of thiosemicarbazone derivatives at 25 °C using equivalent circuits presented in Fig. 4

Inhibitor type		R_s (Ω cm^2)	R_1 (Ω cm^2)	CPE_1 ($\mu\Omega^{-1}$ cm^{-2} S^n)	n_1	R_2 (Ω cm^2)	n_2	CPE_2 (mΩ^{-1} cm^{-2} S^n)	L (H cm^2)	R_3 (Ω cm^2)	Π%
	Blank	0.6	32	15.7	0.89	1.7	0.75	5.9	–	–	–
p-Methoxy thiosemicarabzone	10^{-4}	1.3	42.4	27	0.81	3.1	0.88	8	8	3	28.2
	10^{-3}	1.5	73.5	20	0.78	5.2	0.88	7	7	3.5	58.5
	5×10^{-3}	1.2	142	15	0.77	7.3	0.87	6.7	6	5.5	78.4
	10^{-2}	1.8	194	8	0.78	10.2	0.85	9	5	6.1	84.6
p-Methyl thiosemicarabzone	10^{-4}	1.3	54	30	0.69	11.2	0.89	12	10	9	44.6
	10^{-3}	1.3	88.7	22	0.73	13.1	0.83	11	8	10.7	65.8
	5×10^{-3}	1.5	173.5	18	0.77	20.2	0.89	22	7	13.4	82.4
	10^{-2}	1.8	313.2	10	0.79	26.1	0.83	31	6	8.4	90.8
p-Amino thiosemicarabzone	10^{-4}	1.3	55	32	0.75	16	0.85	9.2	–	–	56.3
	10^{-3}	1.6	78	23	0.73	38	0.81	8.1	–	–	73.5
	5×10^{-3}	1.4	199	20	0.79	63	0.78	7.3	–	–	88.2
	10^{-2}	1.8	369	12	0.75	156	0.77	3.2	–	–	94.3

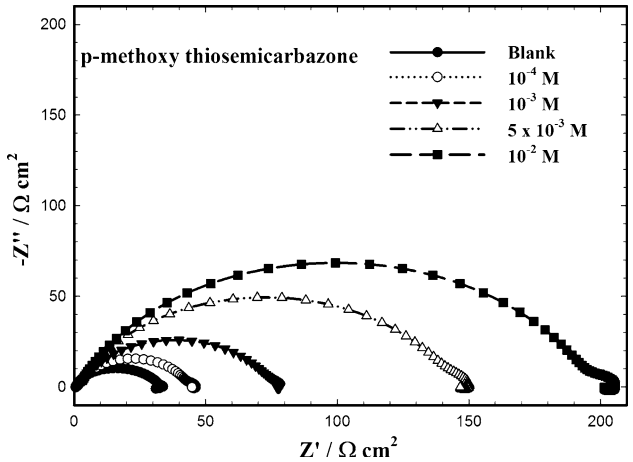

Fig. 1 Nyquist plots for nickel in 1.0 M HNO_3 solutions in the absence and presence of various concentrations of *p*-methoxyacetophenone thiosemicarbazone at 25 °C

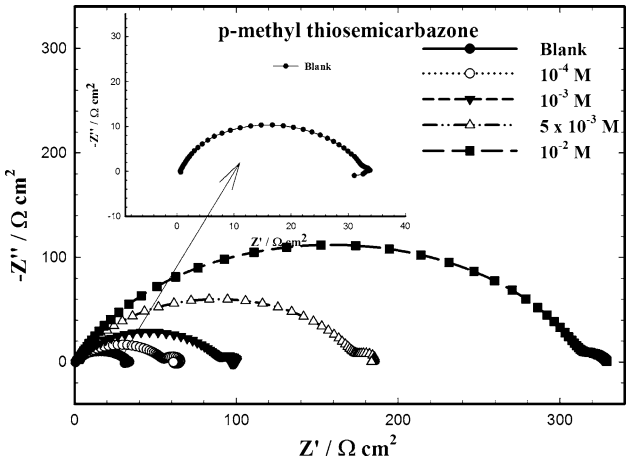

Fig. 2 Nyquist plots for nickel in 1.0 M HNO_3 solutions in the absence and presence of various concentrations of *p*-methylacetophenone thiosemicarbazone at 25 °C

probably due to the consequence of the layer stabilization byproducts of the corrosion reaction on the electrode surface involving inhibitor molecules and their reactive products [19]. It may also be attributed to the re-dissolution of passivated surface. On the other hand, as is seen, the HF capacitance loops in Figs. 1, 2, and 3 enlarge as the increase of methoxy and methyl derivatives concentrations, respectively. It means that the inhibition efficiency is proportional to the increment of inhibitor concentration. Namely, the greater the inhibitor concentration, the higher the inhibition efficiency.

As seen from Figs. 1, 2, and 3, the Nyquist plots semicircle diameters are increased by increasing the inhibitor concentration, indicating that the corrosion is mainly a charge transfer process [20]. A loop is also seen at low frequencies which could be arising from the adsorbed intermediate products on the nickel surface [21]. It is worth noting that the change in the concentration of thiosemicarbazone derivatives did not alter the style of the impedance curves, suggesting a similar mechanism of inhibition is involved.

In case of amino derivative (see Fig. 3), two capacitive loops with two time constants are appeared, first at HF with high polarization resistance (R_1) and the other at LF with small polarization resistance (R_2) appear. The total polarization resistance R_p equals ($R_1 + R_2$). Impedance spectra of amino derivative shown in Fig. 3 can be interpreted by using two time constants model as presented in Fig. 4. In case of amino derivative, the first time constant was shown at HF and was related to an external porous layer, whereas

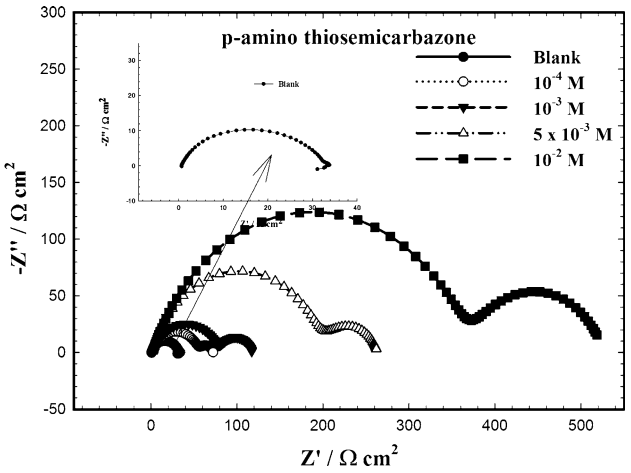

Fig. 3 Nyquist plots for nickel in 1.0 M HNO_3 solutions in the absence and presence of various concentrations of *p*-aminoacetophenone thiosemicarbazone at 25 °C

the second time constant, at lower frequencies, was attributed to a more resistive internal layer. In this case, the transfer function is the sum of the corresponding layer impedance [22].

$$\overline{Z}(S)^{-1} = \overline{Y}(S) = \theta\overline{Y_{\mathrm{L}}}(S) + (1-\theta)\overline{Y_{\mathrm{corr}}}(S) \tag{2}$$

where $\overline{Y_{\mathrm{L}}}(S)$ is the layer admittance and $\overline{Y_{\mathrm{corr}}}(S)$ denotes the admittance of the corrosion process which occurs at the nickel/nitric acid interface at the bottom of the "virtual pores" within the film [22].

Figure 4 shows the equivalent circuit models used to fit the experimental impedance data of nickel in 1.0 M HNO_3 containing inhibitors, in this case R_s refers to the solution resistance, CPE the constant phase element, R the polarization resistance, L the inductance. Inductivity L may be correlated with a slow LF intermediate process [23]. It should be noticed that the depression of the large semicircles (i.e., rather than perfect semicircles) in the complex impedance plane of the Nyquist plots, with the centre under the real axis, appears in Fig. 4. Deviation of this kind, often referred to as frequency dispersion, was attributed to roughness and inhomogeneities of the solid surface. Therefore, a constant phase element (CPE) instead of a capacitive element is used in Fig. 4 to get a more accurate fit of experimental data sets using generally more complicated equivalent circuits. The impedance, Z, of CPE has the form [24]:

$$Z_{\mathrm{CPE}} = [Q(j\omega)]^{-n} \tag{3}$$

where Q is the CPE constant, which is a combination of properties related to the surface and electro-active species, $j^2 = -1$ the imaginary number, ω the angular frequency and n is a CPE exponent which can be used as a measure of the heterogeneity or roughness of the surface. Depending on the value of n, CPE can represent resistance ($n = 0$, $Q = 1/R$), capacitance ($n = 1$, $Q = C$), inductance ($n = -1$, $Q = 1/L$) or Warburg impedance ($n = 0.5$, $Q = W$) [18].

Table 1 contains all the impedance parameters obtained from the simulation of experimental impedance data for methyl, methoxy and amino derivatives, including R_s, R_1, R_2, R_3, R_4, L and CPEs (for the fitting of Q, $n = 0.7$–0.89). The inhibition efficiency ($\Pi\%$) is calculated from the following equation [25]:

$$\Pi\% = \left(1 - \frac{R_{\mathrm{o}}}{R}\right) \times 100 \tag{4}$$

where R_{o} and R represents the uninhibited and inhibited polarization resistance (intersection of the LF inductive loop with x-axis in case of methoxy and methyl derivatives and intersection of the LF capacitive loop with x-axis in case of amino derivative), respectively. It can be seen from Table 1 that, with the increase of inhibitor concentrations, the inhibition efficiencies increase noticeably, especially the situation of increasing concentration of amino derivative. At the

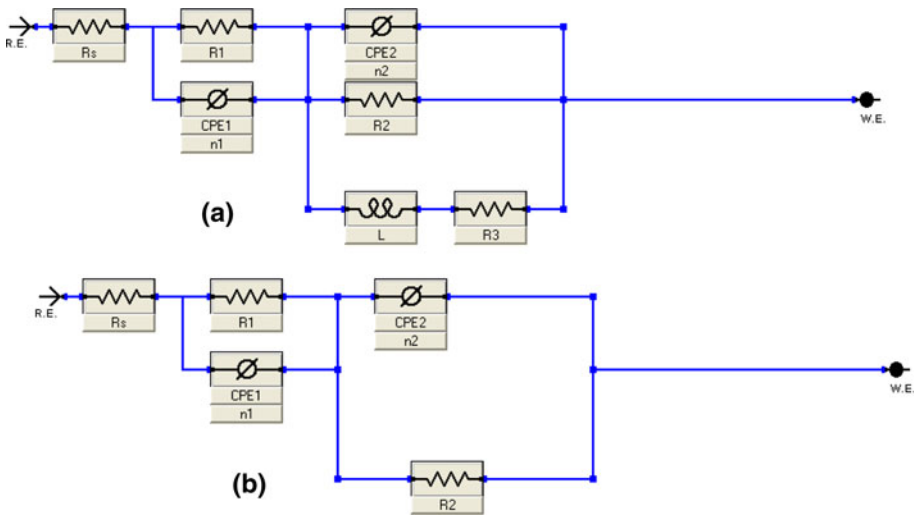

Fig. 4 Equivalent circuits used to model impedance data for nickel in 1.0 M HNO_3 solutions: **a** equivalent circuit for methoxy and methyl derivatives, **b** equivalent circuit for amino derivative

same concentration of inhibitors, the inhibition efficiency of these inhibitors is in the order: amino > methyl > methoxy.

4.2 Potentiodynamic polarization

The polarization curves of nickel electrode in aerated 1.0 M HNO_3 solutions with varying concentrations of thiosemicarbazone derivatives at 25 °C ± 1 are shown in Figs. 5, 6, and 7.

It is obvious that the nickel electrode immersed in nitric acid solution displays a cathodic region of Tafel behavior. However, the anodic polarization curve does not display an extensive Tafel region, instead it shows a plateau that goes with primary passivity, and arises after oxygen evolution [26]. The existence of passivation in conjunction with a dissolution reaction does not result in a well-defined experimental anodic Tafel region. Therefore, due to absence of linearity in anodic branch, accurate evaluation of the anodic Tafel slope (β_a) by Tafel extrapolation of the anodic branch is impossible [27–30]. There is, therefore an uncertainty and source of error in the numerical values of the anodic Tafel slope (β_a); the reason why we did not introduce β_a values recorded by the software. It has been shown that in the Tafel extrapolation method, use of both the anodic and cathodic Tafel regions is undoubtedly preferred over the use of only one Tafel region [31]. However, the corrosion rate can also be determined by Tafel extrapolation of either the cathodic or anodic polarization curve alone. If only one polarization curve alone is used, it is generally the cathodic curve which usually produces a longer and better defined Tafel region in Figs. 5, 6, and 7. Detailed description of the method of determination of corrosion current density by this method has been presented elsewhere [32, 33].

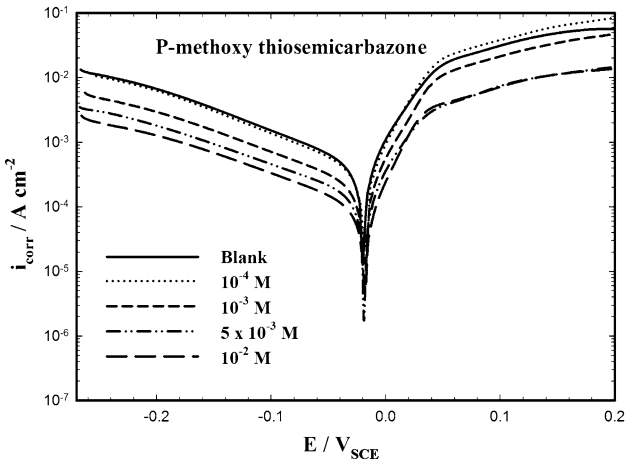

Fig. 5 Anodic and cathodic polarization curves for nickel in 1.0 M HNO_3 solutions in the absence and presence of various concentrations of *p*-methoxyacetophenone thiosemicarbazone at 25 °C

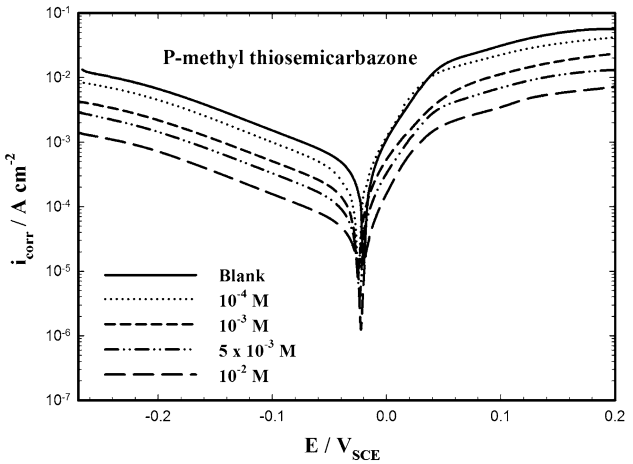

Fig. 6 Anodic and cathodic polarization curves for nickel in 1.0 M HNO_3 solutions in the absence and presence of various concentrations of *p*-methylacetophenone thiosemicarbazone at 25 °C

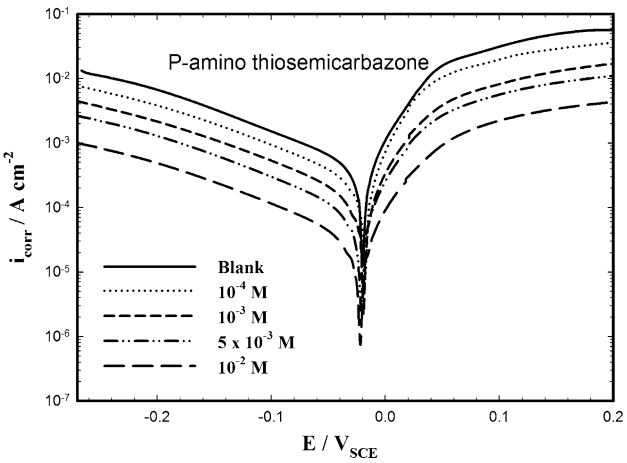

Fig. 7 Anodic and cathodic polarization curves for nickel in 1.0 M HNO_3 solutions in the absence and presence of various concentrations of *p*-aminoacetophenone thiosemicarbazone at 25 °C

Although the anodic dissolution of nickel in nitric acid is well described in the literature [34–36], there is no means agreement either on the mechanism of passivation of nickel or on the composition and thickness of the passive layer [37]. Generally, the important feature is that the nature of the anion of the electrolyte is a determining parameter in the anodic dissolution of nickel [26]. Analyzing the form of polarization curves in Figs. 5, 6, and 7, we can see some different phases of polarization. First, the anodic polarization curve corresponds to the electrochemical generation of nickel oxide and/or nitrates. Several reaction schemes for interpreting the anodic dissolution/passivation of nickel in dilute nitric acid have been presented in the literature [11, 37, 38]. All the electron and mass transfers are made through the intermediate of adsorbed species at the reactive interface; so we propose

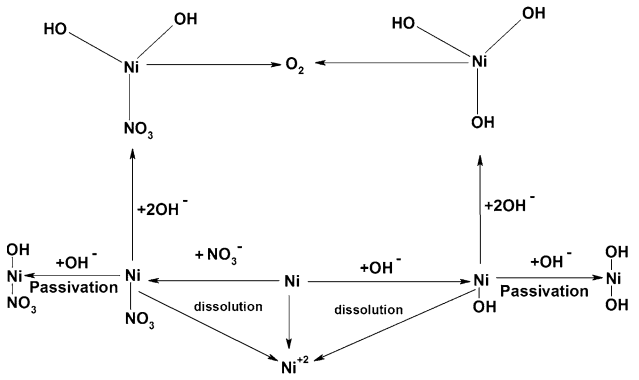

Fig. 8 Path of all possible reactions on the anodic plateau in Figs. 5, 6, and 7 [11, 37, 38]

only one general model where all the reactions may be produced by anion (NO_3^- or OH^-). Figure 8 presents a scheme of all the reactions: on a nickel atom one anion NO_3^- or OH^- may be adsorbed and the surface active anions are believed to participate directly in the dissolution process by adsorption at the nickel surface.

As an example, the dissolution of nickel in presence of nitrate anion ($A = NO_3^-$) can be described by the following set of equations [26], where k_1 and k_2 are rate constants

$$Ni + A^- \xrightarrow{k_1} Ni - A_{ads} + e^- \quad (5)$$

$$Ni - A_{ads} \xrightarrow{k_2} Ni - A_{ads}^+ + e^- \quad (6)$$

$$Ni - A_{ads}^+ \rightarrow Ni^{+2} + e^- \quad (7)$$

Equation 7 is a chemical reaction, whereas Eqs. 5 and 6 are electrochemical reactions which involve the adsorbed intermediate species $Ni–A_{ads}$; this intermediate occupies a fraction θ of the electrode area.

On the other hand, it is known [38] that the series of the cathodic reactions of the reduction of nitric acid occurs in the following way:

$$NO_3^- \rightarrow NO_2 \rightarrow NO_2^- \rightarrow NO \rightarrow N_2 \rightarrow \ldots \quad (8)$$

Some authors show that the reduction of nitric acid on nickel electrode can even lead to the formation of ammonia [39].

The influence of the anodic and cathodic reactions on the behavior of nickel in nitric acid has been investigated by addition of thiosemicarbazone derivatives to the solution. Addition of thiosemicarbazone derivatives retards the anodic dissolution and cathodic reduction reactions that occur on nickel surface in 1.0 M HNO_3. Thiosemicarbazone derivatives destroy completely nitrous acid which is always present in small amounts in nitric acid [40] and which increases by the reduction of nitric acid. The values of the corrosion current density (i_{corr}) for nickel corrosion reaction without and with thiosemicarbazone derivatives were determined by extrapolation of the cathodic Tafel lines to the corrosion potential (E_{corr}). Table 2 represents the influence of thiosemicarbazone derivatives on the corrosion kinetic parameters. As it can be seen form Figs. 5, 6, and 7, the anodic and cathodic reactions are affected. Thiosemicarbazone derivatives are thus mixed-type inhibitors, meaning that the addition of these compounds to nitric acid solutions reduces the anodic dissolution of nickel, corresponding to a noticeable decrease in the current densities of the passivation plateau, and also retards the cathodic reactions that occurs on the nickel surface.

Table 2 Electrochemical kinetic parameters, inhibition efficiencies and rates of corrosion associated with Tafel polarization measurements recorded for nickel in 1.0 M HNO_3 solutions without and with various concentrations of the three selected thiosemicarbazone derivatives acids at 25 °C

Inhibitor type	[Inhib] (M)	β_c (mV dec^{-1})	$-E_{corr}$ (mV (SCE))	i_{corr} (μA cm^{-2})	Ψ%	Corrosion rate (mpy)
	Blank	169.1	19.8	527	–	223.7
p-Methoxy thiosemicarabzone	10^{-4}	157.1	18	402.0	23.7	170.7
	10^{-3}	169.5	18.5	234.0	55.6	99.19
	5×10^{-3}	177.6	19	161.5	69.3	68.47
	10^{-2}	179.7	118.3	115.0	78.2	48.79
p-Methyl thiosemicarabzone	10^{-4}	166.6	25.0	355.0	32.6	150.8
	10^{-3}	177.7	25.5	204.0	61.3	86.51
	5×10^{-3}	169.4	24.0	119.0	77.4	50.53
	10^{-2}	166.1	22.1	54.3	89.7	23.07
p-Amino thiosemicarabzone	10^{-4}	171.0	18.8	297.0	43.6	126.1
	10^{-3}	171.5	19.1	173.0	67.2	73.4
	5×10^{-3}	167.3	21.4	98.4	81.3	44.78
	10^{-2}	171.4	22.3	40.1	92.4	17.1

Electrochemical parameters associated with polarization measurements, such as corrosion potential (E_{corr}), corrosion currents densities (i_{corr}) and cathodic Tafel slope (β_c), are listed in Table 2 as a function of thiosemicarbazone derivatives concentration. As it can be seen, the corrosion potential (E_{corr}) has no definite shift and (i_{corr}) decreases when the concentration of thiosemicarbazone derivatives is increased. Absence of significant change in the cathodic Tafel slope (β_c) in the presence of thiosemicarbazone derivatives indicates that the corrosion mechanism is not changed after adding the thiosemicarbazone derivatives, and the inhibition effect is due to simple adsorption. These findings also indicate that the cathodic reactions are under activation-controlled and the addition of thiosemicarbazone derivatives does not affect the mechanism of the corrosion process [41].

It follows from the data of Table 2 that, at a 25 °C, the inhibition efficiency increases with increasing thiosemicarbazone derivatives concentrations. It is seen that thiosemicarbazone derivatives has inhibiting properties at all studied concentrations and the values of inhibition efficiencies, Ψ% increase as the thiosemicarbazone derivatives concentrations increase.

The percentage of inhibition efficiency (Ψ%) were calculated using the following equation:

$$\Psi\% = \left(1 - \frac{i_{corr}}{i^{o}_{corr}}\right) \times 100 \quad (9)$$

where i^{o}_{corr} and i_{corr} are corrosion current densities in the absence and presence of inhibitors, respectively. From the results in Table 2, it can be observed that the values of corrosion current density (i_{corr}) of nickel in the inhibitor-containing solutions were lower than those for the inhibitor-free solution. The corrosion current densities at all inhibitor concentrations are decreased in the order of amino > methyl > methoxy.

4.3 Computational study

Molecular modeling studies give indications of a strong molecular attraction to the metal to better understand the performance mechanism for the thiosemicarbazone derivatives. The modeling studies were designed to examine this theory by predicting the inhibitor–surface interactions that lead to optimal molecular binding at the nickel surface.

Monte Carlo simulation, molecular dynamics were performed on a system comprising thiosemicarbazone derivatives, solvent molecules and Ni(111) surface. Each thiosemicarbazone derivative is placed on the Ni(111) surface, optimize and then run quench molecular dynamics. Total energy, average total energy, Van der Waals energy, electrostatic energy and intramolecular energy for the studied system are presented in Fig. 9 (representative example for optimization energy of Ni(111)/solvent/methyl derivative system). Monte Carlo docking was done on each of the 100 conformations, and each of the docked structures was energetically relaxed.

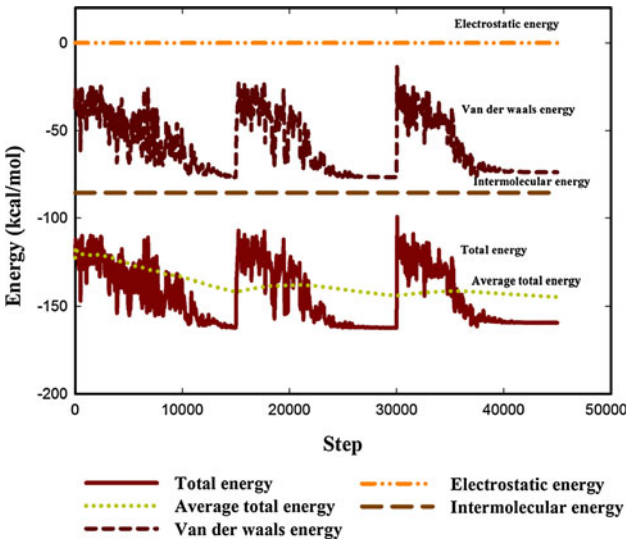

Fig. 9 Total energy distribution for methyl derivative/solvent/Ni(111) system

The Monte Carlo simulation process tries to find the lowest energy for the whole system. The structures of the adsorbate components are minimized until they satisfy certain specified criteria. The outputs and descriptors calculated by the Monte Carlo simulation are presented in Table 3. The parameters presented in Table 3 include total energy of the substrate–adsorbate configuration. The total energy is defined as the sum of the energies of the adsorbate components, the rigid adsorption energy, and the deformation energy. In this study, the substrate energy (nickel surface) is taken as zero. Also, adsorption energy reports energy released (or required) when the relaxed adsorbate components are adsorbed on the substrate.

The adsorption energy is defined as the sum of the rigid adsorption energy and the deformation energy for the adsorbate components. The rigid adsorption energy, reports the energy, in kcal mol^{-1}, released (or required) when the unrelaxed adsorbate components (i.e., before the geometry optimization step) are adsorbed on the substrate. The deformation energy, reports the energy released when the adsorbed adsorbate components are relaxed on the substrate surface. Table 3 shows also, (dE_{ads}/dN_i) which defines the energy of substrate–adsorbate configurations where one of the adsorbate components has been removed. As can be seen from Table 3, the amino derivative gives the maximum adsorption energy found during the simulation process (−76.5 kcal mol^{-1}). High values of adsorption energy confirm experimental results and explain why the amino derivative gives the highest inhibition efficiency.

Table 3 Outputs and descriptors calculated by the Mont Carlo simulation for adsorption of thiosemicarbazone derivatives on Ni(111)

Inhibitor	Total energy (kcal mol^{-1})	Adsorption energy (kcal mol^{-1})	Rigid adsorption energy (kcal mol^{-1})	Deformation energy (kcal mol^{-1})	dE_{ad}/dN_i (kcal mol^{-1})	Calculated binding energy (kcal mol^{-1})
p-Methoxy thiosemicarabzone	−158.1	−84.4	−86.33	1.9	−84.4	322
p-Methyl thiosemicarabzone	−163.8	−78.25	−78.6	0.4	−78.25	356
p-Amino thiosemicarabzone	−150.3	−76.5	−80.36	3.7	−76.5	411

Table 4 HOMO and LUMO energies, HOMO–LUMO gap (ΔE) and dipole moment μ for the three thiosemicarbazone derivatives obtained in the gas phase and in the presence of water, respectively

Inhibitor	E_{HOMO} (eV)	E_{LUMO} (eV)	$\Delta = E_{LUMO} - E_{HOMO}$ (eV)	μ (D)
p-Methoxy thiosemicarabzone	−8.55	−0.941	7.609	6.96
	−8.88	−1.1	7.78	7.81
p-Methyl thiosemicarabzone	−8.59	−9.975	7.615	6.76
	−8.78	−0.99	7.79	7.01
p-Amino thiosemicarabzone	−8.54	−0.9057	7.635	6.521
	−8.61	−0.996	7.614	6.81

The "total energy" of a molecule presented in Table 3 refers to the energy of a specific arrangement of atoms. The zero energy reference is taken to be the infinite separation of all electrons and nuclei, so the total energy is generally negative, corresponding to a bound state.

The effectiveness of an inhibitor can be related to its electronic and spatial molecular structure. Also, there are certain quantum-chemical parameters that can be related to the interactions of metal-inhibitor, these are: the HOMO energy that is often associated with the capacity of a molecule to donate electrons, the energy gap ΔE (the lower values of energy gap, the better corrosion inhibition), and the dipole moment because low values will favor the accumulation of inhibitor molecules on the metallic surface. A good correlation between the rate of corrosion and E_{HOMO}, as well as with energy gap ($\Delta E = E_{LUMO} - E_{HOMO}$) has been found in previous works [42, 43].

In Table 4, several theoretical parameters were calculated in liquid as well as in gas phase. The calculated parameters in gas phase as well as in the presence of a solvent do not exhibit important differences. The solvent in these calculations regarded as a continuous of uniform dielectric constant (ε) and the solute is placed in a cavity within it [44]. The HOMO energy can indicate the disposition of the molecule to donate electrons to an appropriated acceptor with empty molecular orbitals (d orbital in nickel). Also, an increase in the values of E_{HOMO} can facilitate the adsorption, and therefore improved inhibition efficiency results [45]. The corrosion rate must decrease with increases in HOMO energy (less negative) [42], therefore an increase in the corrosion inhibition is present (see Table 4).

Low values of the energy gap (ΔE) will provide good inhibition efficiencies, because the excitation energy to remove an electron from the last occupied orbital will be low [46]. The results show that the amino derivative has the lowest energy gap; this agrees with the experimental results that amino derivative could have better performance as a corrosion inhibitor (see Table 4).

Figure 10 shows the predicted adsorption density of thiosemicarbazone derivatives on the Ni(111) substrate. As can be seen from Fig. 10, that the amino derivative shows the highest ability to adsorb on Ni surface with highest adsorption density. Also, it has the highest binding energy to Ni surface as seen in Table 3. Adsorption density calculation presented in Fig. 10 is identified by carrying out a Monte Carlo search of the configurational space of the substrate–adsorbate system as the temperature is slowly decreased. This process is repeated to identify further local energy minima. During the course of the simulation, adsorbate molecules are randomly rotated and translated around the substrate. The configuration that results from one of these steps is accepted or rejected according to the selection rules of the Metropolis Monte Carlo method.

4.4 Mechanism of adsorption

Three modes of adsorption can be identified for the adsorption of thiosemicarbazone derivatives. These modes of adsorptions include physical, chemical and adsorption through hydrogen bonding. Physical adsorption is the result of electrostatic attractive forces between the cationic form of thiosemicarbazone derivatives and the electrically charged nickel surface. Chemisorption process involves charge sharing or charge-transfer from the lone pairs of electrons in the thiosemicarbazone derivatives to the vacant

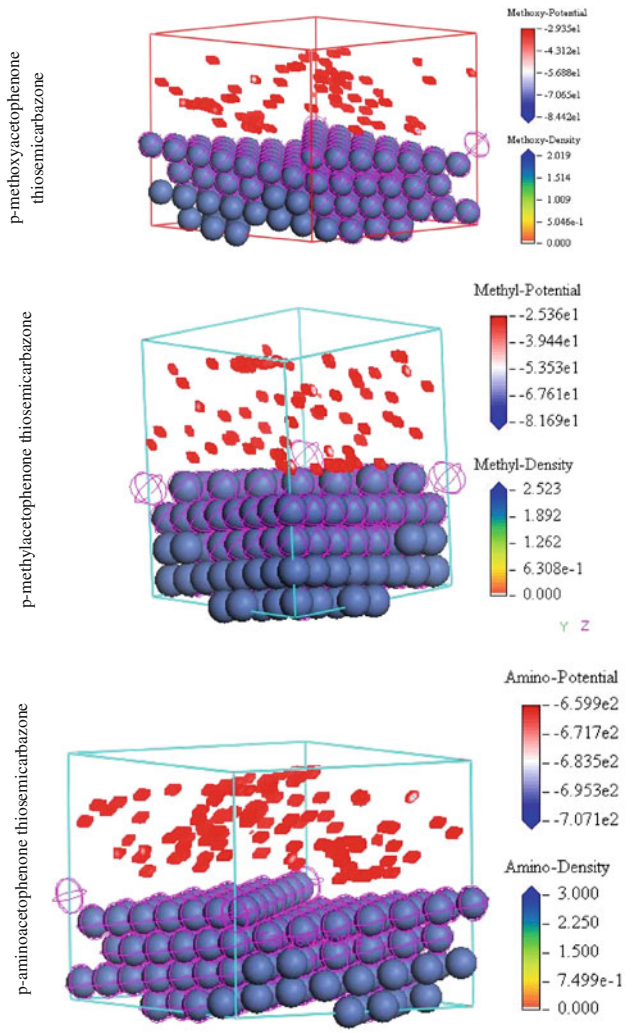

Fig. 10 The adsorption density of thiosemicarbazone derivatives on the Ni(111) substrate

d-orbital in the nickel surface to form a coordinate type of a bond.

Literature survey shows that few investigations have shown that adsorption could also occur through hydrogen bonding [47, 48].

Physical adsorption might be occur between the negative nickel surface and the protonated thiosemicarbazone derivatives. In addition to the physical adsorption, there should be chemical adsorption owing to the coordinate bonds formed between the lone electron pairs of the N-atom in thiosemicarbazone derivatives and the empty orbits of nickel atoms which enhanced the combination between the thiosemicarbazone derivatives molecules and electrode surface. The adsorption monolayer of thiosemicarbazone derivatives became compact and adherent to the nickel surface with increasing its concentration, so the cathodic reduction and anodic dissolution reaction were inhibited extremely.

In the passive region where the surface of the nickel electrode is covered by oxide layer with different composition [37]. This layer agrees with the finding of Hoare and Wiese [49] about the formation of NO_2 film which transforms slowly to NiO. On the other hand, it may be possible, according to Korte [50], that in the beginning of the repassivation process $Ni(NO_3)_2{\cdot}4H_2O$ forms which changes to NO_2 and NiO, respectively.

The presence of oxide layer on the nickel surface encourages the adsorption of the thiosemicarbazone derivatives on the nickel surface via H-bonding.

Adsorption in this case is assisted by hydrogen bond formation between thiosemicarbazone derivatives and oxidized surface species. This type of adsorption should be more prevalent for protonated N-atom, because the positive charge on N-atom is conductive to the formation of hydrogen bonds. Unprotonated N-atom may adsorb by direct chemisorption or by hydrogen bonding to a surface oxidized species. The extent of adsorption by the respective modes depends on the nature of the metal surface. Adsorption by direct chemisorption, for unprotonated N-atom, on an exposed nickel atom is more probable in the active region. In this region, although the unprotonated N-atom can interact with oxidized metal and the corrosion intermediates by hydrogen bonding, little is contributed to corrosion inhibition because corrosion intermediates and surface oxides could not form a stable compact layer on the metal surface. Effective inhibition is predominantly provided by the direct coordination of unprotonated N-atom to metal atoms. In the passive region where the nickel surface is covered by an adherent oxide protective layer, the direct coordination of nitrogen to an exposed metal atom is a remote event. Protonated and unprotonated N-atoms are adsorbed onto nickel through hydrogen bond formation. These results confirm the importance of hydrogen bonding in effective corrosion inhibition in the passive region.

5 Conclusions

The three selected thiosemicarbazone derivatives were found to be effective inhibitors for nickel corrosion in 1.0 M HNO_3 solutions. Understanding adsorption phenomena is of key importance in corrosion problems. Computational studies help to find the most stable adsorption sites for a broad range of materials. This information can help to gain further insight about corrosion system, such as the most likely point of attack for corrosion on a surface, the most stable site for inhibitor adsorption and the binding energy of the adsorbed layer. With such knowledge at hand, we will be able to better guide subsequent screening experiments for corrosion inhibitors that save both time and money.

Acknowledgments Author is grateful for Taif University and the center of research excellence in corrosion for their financial support. The experimental work was supported by Taif university project # 1-431-636 and the theoretical calculations which added to the manuscript in the revised version were supported by the center of research excellence in corrosion located at King Fahd University, Project # CR-03-2010 titled "Designing new corrosion inhibitors by QSAR and Molecular Dynamics Approaches".

References

1. Ramachandran S, Tsai BL, Blanco M, Chen H, Tang YC, Goddard WA (1997) J Phys Chem A 101:83
2. Khaled KF (2008) Electrochim Acta 53:3484
3. Kornherr A, Hansal S, Hansal WEG, Besenhard JO, Kronberger H, Nauer GE, Zifferer G (2003) J Chem Phys 119:9719
4. Selembo PA, Merrill MD, Logan BE (2009) J Power Sources 190:271
5. Grant JC (1975) Nickel–cadmium battery application engineering handbook, 3rd edn. General Electric Company, Gainesville
6. Ahn KH, Song KG, Cha HY, Yeom IT (1999) Desalination 122:77
7. McGeough JA, Leu MC, Rajurkar KP, De Silva AKM, Liu Q (2001) CIRP Ann Manuf Technol 50:499
8. Rossi S, Deflorian F, Venturini F (2004) J Mater Process Technol 148:301
9. Gilli G, Borea P, Zucchi F, Trabanelli G (1969) Corros Sci 9:673
10. Khaled KF (2011) Mater Chem Phys 125:427
11. Kumar A, Patnaik SK, Singh MM (1998) Mater Chem Phys 56:243
12. Khaled KF (2008) J Appl Electrochem 38:1609
13. Khaled KF (2010) Electrochim Acta 55:5375
14. Barriga J, Coto B, Fernandez B (2007) Tribol Int 40:960
15. Sun H, Ren P, Fried JR (1998) Comput Theor Polym Sci 8:229
16. Khaled KF (2009) J Solid State Electrochem 13:1743
17. Khaled KF, Fadl-Allah SA, Hammouti B (2009) Mater Chem Phys 117:148
18. Morad MS (2000) Corros Sci 42:1307
19. Kelly EJ (1965) J Electrochem Soc 112:125
20. Bentiss F, Lagrenee H, Traisnel M, Hornez JC (1999) Corros Sci 41:789
21. Solmaz R, Kardaş G, Çulha M, Yazici B, Erbil M (2008) Electrochim Acta 53:5941
22. Juttner K (1990) Electrochim Acta 35:1501
23. Gojic M (2001) Corros Sci 43:919
24. Ramelt U, Reinhard G (1990) Electrochim Acta 35:1045
25. Khaled KF, Hackerman N (2003) Electrochim Acta 48:2715
26. Jouanneau A, Keddam M, Petit MC (1981) Electrochim Acta 21:287
27. Jones DA (1992) Principles and prevention of corrosion. Macmillan, New York
28. Flitt HJ, Schweinsberg DP (2005) Corros Sci 47:3034
29. Mansfeld F (2005) Corros Sci 47:3178
30. Flitt HJ, Schweinsberg DP (2005) Corros Sci 47:2125
31. McCafferty E (2005) Corros Sci 47:3202
32. Khaled KF (2008) Appl Surf Sci 255:1811
33. Amin MA, Khaled KF, Fadllalah SA (2010) Corros Sci 52:140
34. Kabanov BN (1968) Electrochim Acta 19:13
35. Kolotyrkin T, Golovina GV, Florianovich GM (1963) Dokl Akad Nauk SSSR 198:1106
36. Schwabe K, Ebersbach U, Seinbrock W (1972) Electrochim Acta 17:957
37. Stupnišek-Lisac E, Karšulin M (1984) Electrochim Acta 29:1339
38. Pascal P (1956) Nouveau traite de chimie mineral. X masson, Paris
39. Miroljubov N, Razigrajev VP, Pisarenko TA (1973) Phys Chim 213:1361
40. Kazanjian AR, Miner FJ, Hagan AK, Berry JW (1973) Trans Faraday Soc 66:2192
41. Said F, Souissi N, Es-Salah K, Hajjaji N, Triki E, Srhiri A (2007) J Mater Sci 42:9070
42. Sastri VS, Perumareddi JR (1997) Corros Sci 53:617
43. Lukovits I, Kálmán E, Zucchi F (2001) Corrosion 57:3
44. Foresman JB, Frisch Æ (1996) Exploring chemistry with electronic structure methods, 2nd edn. Gaussian, Inc., Pittsburgh
45. Khalil N (2003) Electrochim Acta 48:2635
46. Bentis F, Traisnel M, Vezin H, Hildebrand HF, Lagrenée M (2004) Corros Sci 46:2781
47. Incorvia MJ, Contarini S (1989) J Electrochem Soc 136:2493
48. Karman FH, Felhosi I, Kalman E, Cserny I, Kover L (1998) Electrochim Acta 43:69
49. Hoare JP, Wiese ChR (1975) Corros Sci 15:15
50. Korte F (1974) Methodicum chimicum, vol 1. Academic Press, New York, p 357